Soft Matter

Accepted Manuscript

ROYAL SOCIETY OF CHEMISTRY

www.rsc.org/softmatter

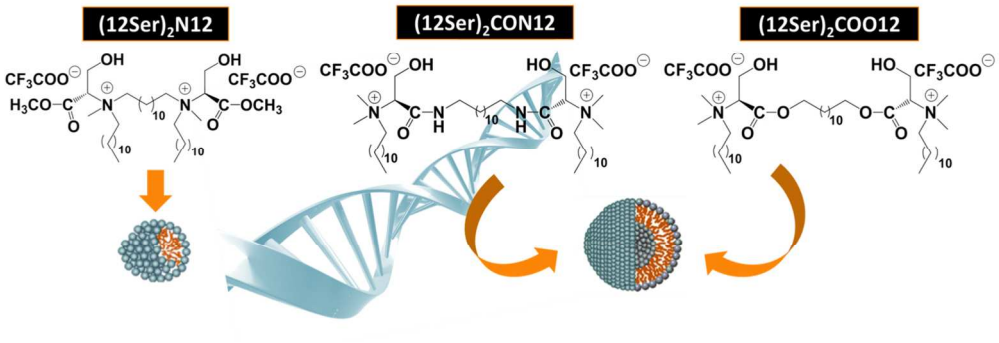

529x203mm (72 x 72 DPI)

Journal Name

RSCPublishing

ARTICLE

Serine-based Gemini Surfactants with Different Spacer Linkages: From Self-Assembly to DNA Compaction

Cite this: DOI: 10.1039/xoxxoooooox

Received ooth January 2014,
Accepted ooth January 2014

DOI: 10.1039/xoxxoooooox

www.rsc.org/

Sandra G. Silva, Isabel S. Oliveira, Maria L. C. do Vale and Eduardo F. Marques*

Cationic gemini surfactants have a strong potential as compaction agents of nucleic acids for efficient non-viral gene delivery. In this work, we present the aggregation behavior of three novel cationic serine-based gemini surfactants as well as their ability to compact DNA per se and mixed with a helper lipid, 1,2-dioleoyl-*sn*-glycero-3-phosphoethanolamine (DOPE). All the surfactants have a 12-12-12 configuration, i.e. two main 12-carbon alkyl chains linked to the nitrogen atom of the amino acid residue and a 12 methylene spacer, but they differ in the nature of the spacer linkage: for $(12Ser)_2N12$, an amine bond; for $(12Ser)_2CON12$, an amide bond; and for $(12Ser)_2COO12$, an ester bond. Interestingly, while the amine-based gemini aggregates into micelles, the amide and ester ones spontaneously form vesicles, which denotes a strong influence of the type of linkage on the surfactant packing parameter. The size, ζ-potential and stability of the vesicles have been characterized by light microscopy, cryogenic scanning electron microscopy (cryo-SEM) and dynamic light scattering (DLS). The interaction of the gemini aggregates with DNA, at different charge ratios and in absence and presence of DOPE has been studied by DLS, fluorescence spectroscopy and cryo-SEM. All the compounds are found to efficiently compact DNA (complexation > 90 %), but relevant differences are obtained in terms of size, ζ-potential and stability of the lipoplexes formed. Results are rationalized in terms of headgroup differences and type of aggregates present prior to DNA condensation.

1. Introduction

Self-assembled amphiphile-based nanocarriers constitute one of the most important strategies to build up smart systems for the controlled delivery of biomolecules in the human body.[1-5] In the last decades, cationic gemini surfactants have been investigated in the context of the development of non-viral vectors for gene therapy.[6-11] Their lower *cmc* values compared to those of the monomeric analogues allow gemini surfactants to self-assemble more readily in aqueous environments and bind or compact DNA with higher efficiency at lower concentrations.[6-11] The enhanced performance of gemini surfactants is attributed to the versatility provided by tailor-made variations in their molecular structure, namely in the length and nature of the lipophilic chains and spacer groups, and in the chemical nature of the headgroups.[12-16]

Bis-quaternary ammonium salts (*bis*-quats) have been by far the most common type of gemini surfactants investigated for bio-related applications.[8,10,15,17-21] Their use is, however, somewhat limited by their toxicity profiles.[22,23] To overcome this issue, a great deal of effort has been devoted to the development of increasingly biofriendly and biocompatible amphiphiles. Thus, in recent years, gemini surfactants incorporating natural structural motifs, like carbohydrates[24-27] and amino acids[28-32] have been designed and synthesized, with many of them showing indeed attractive biological features.

Cationic gemini surfactants are capable of binding DNA, forming complexes known as lipoplexes. The properties of the lipoplexes depend on the aggregate size of the surfactant, the ionic strength of the medium, the surfactant and DNA concentration, the surfactant/DNA charge ratio and the order of addition of the components.[33-36] The efficiency of DNA complexation may be improved by addition of helper lipids, which induce an increase in counterion dissociation from the cationic surfactant aggregate, allowing for a more effective interaction of the DNA phosphate groups with the cationic charges. Furthermore, helper lipids may enhance the stability of the lipoplexes, reduce the toxicity of cationic surfactants and help in membrane perturbation and fusion, thus increasing the transfection efficiency.[37,38] The zwitterionic lipid DOPE, 1,2-dioleoyl-*sn*-glycero-3-phosphoethanolamine, is often used as helper lipid. Upon endosomal compartmentalization, DOPE undergoes protonation and is thought to self-assemble into non-

bilayer structures, thereby leading to the disruption and destabilization of the endosomal bilayer, which in turn results in the rapid release of DNA into the cytoplasm.[22,39-41]

In the present work, three serine-based gemini surfactants have been used to prepare cationic gene carriers, both individually and in combination with DOPE. The selected compounds possess 12-carbon alkyl chains linked to the nitrogen atoms of the amino acids and a 12-carbon spacer between the amine groups (amine linkage, Fig. 1A) or the carboxylic acid groups (amide or ester bonds, Fig. 1B, 1C). The characterization of the interfacial behavior of the single systems has been initially performed by surface tension. To get further insight into the morphology of the serine and serine/DOPE (1:1 molar ratio) aggregates, light microscopy, cryo-SEM and DLS were used. The efficiency of gemini and gemini/DOPE aggregates to bind/compact DNA at various surfactant-to-DNA charge ratios (CR+/-), in the range of 1.0 – 12, was then followed by DLS and quantified by fluorescence spectroscopy. The lipoplex structure was also investigated by light microscopy and cryo-SEM. As will be shown, the results in terms of DNA complexation ability are very promising for both the neat gemini and mixed gemini/lipid aggregates.

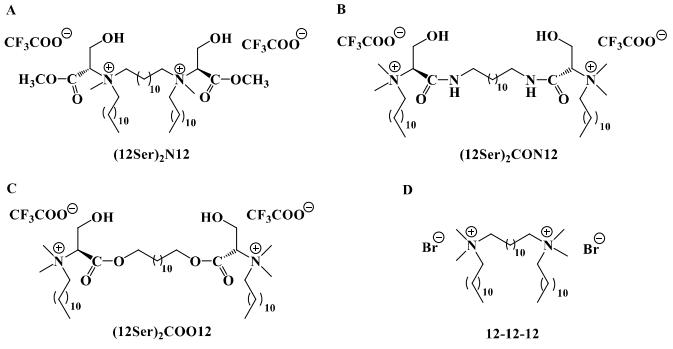

Figure 1. Molecular structure of the serine-based gemini surfactants used in this study: A: $(12Ser)_2N12$ – amine derivative; B: $(12Ser)_2CON12$ – amide derivative and C: $(12Ser)_2COO12$ – ester derivative. For comparison, the structure of the conventional bis-quat gemini 12-12-12 (D) is also shown. The surfactant counterions are trifluoroacetate for A-C and bromide for D.

2. Experimental Section

2.1 Materials

2.1.1 General. The enantiomerically pure (L series) amino acid derivatives H-Ser(OtBu)-OMe and H-Ser(OtBu)-OH were purchased from Bachem (Switzerland) as well as the coupling agents N-[1H-benzotriazol-1-yl)(dimethylamino) methylene]-N-methylmethan-aminiumtetrafluoro borate N-oxide (TBTU) and benzotriazol-1-yloxy-tripyrrolidino-phosphonium hexa--fluorophosphate (PyBOP). The lipid 1, 2-dioleoyl-*sn*-glycero-3-phosphoethanolamine (DOPE) used as helper in DNA compaction studies was supplied by Avanti Polar Lipids (Alabaster). Solvents (p.a. quality) and other chemicals were obtained from Sigma-Aldrich. Thin layer chromatography (TLC) aluminium foil plates covered with silica 60 F254 (0,25 mm) and silica-gel 60 (70-230 mesh ASTM) for preparative column chromatography were from Merck and SDS, respectively. ^{1}H NMR and ^{13}C NMR spectra were recorded on a Bruker Avance III 400 spectrometer. ESI mass spectra were recorded on a Finnigan Surveyor instrument, equipped with mass detector Finnigan LCQ DECA XP MX (Finnigan Corp.San Jose, Calif. USA) and API (Atmospheric Pressure Ionization) using an ESI interface (Electrospray Ionization).

2.1.2 Synthesis. The gemini surfactants A, dodecamethylene *bis*{*N*-(dodecyl)-*N*-[(2-hydroxy-1-methyloxycarbonyl)ethyl]-*N*-(methyl) ammonium} *bis*(trifluoroacetate), B, *N*, *N*'-dodecyl-1,12-diyl *bis* {*N*-[(1*S*)-(1-carbamoyl-2-hydroxyethyl]-*N*-dodecyl-*N*, *N*'-dimethyl ammonium} *bis*(trifluoroacetate), C, *O*, *O*'-dodecyl-1,12-diyl *bis* {*N*-[(1*S*)-(1-oxycarbonyl-2-hydroxy)ethyl]-*N*-dodecyl-*N*, *N*-dimethyl ammonium} *bis*(trifluroacetate) and D, dodecanediyl-α,ω-bis(dodecyl dimethylammonium bromide) were synthesized according to a procedure described by us in previous publications.[29,30]

2.2 Methods

2.2.1 Sample preparation. Samples used in this work were prepared in two different ways. For the phase behavior studies, the compounds were dissolved in Milli-Q ultrapure water and the samples allowed to equilibrate for at least 24 hours at 25 ºC prior to measurements. For the compaction studies, the samples were prepared by thin lipid film hydration. Gemini or gemini/DOPE (1:1 molar ratio) mixtures were dissolved in ethanol and dried under vacuum in a rotary evaporator (50 ºC during 45 minutes). The dried lipid films were then hydrated with Milli-Q water at 35 ºC for 30 min, to a final concentration of 1 mM. This preparation technique yielded a polydisperse population of multilamellar and unilamellar vesicles. In order to make the size distribution more uniform and decrease the polydispersity, a sequential extrusion procedure was performed using a 10 mL stainless steel extruder (Lipex Biomembranes), inserted in a thermostated cell with re-circulating water bath. The vesicle dispersions were initially passed through a 600 nm (10 times) and then through a 200 nm (20 times) polycarbonate filter (Whatman, Nucleopore), under inert atmosphere. The vesicle solutions thus prepared were left undisturbed during 24 hours.

2.2.2 Lipoplex preparation. Lipoplexes were prepared at 25 ˚C by adding increasing aliquots of cationic lipid solutions to 170 µL of salmon sperm DNA solution (10 mM PBS buffer solution), to obtain surfactant/DNA charge ratios from 0.5 to 12. The surfactant-to-DNA charge ratio, CR(+/-), is defined as:

$$CR(+/-) = \frac{2 \times [\text{gemini surfactant}]}{[\text{DNA phosphate groups}]} \quad (1)$$

where the brackets represent molar concentrations of the solutes; note that for each gemini molecule there are two positive charges. The DNA concentration, expressed in mM base pairs, was determined by UV absorbance at 260 nm. The

A260/A280 ratio was always between 1.8 and 1.9, indicating that there was no protein or RNA contamination.[42] The lipoplexes were then incubated at room temperature, under stirring, for 15 min and the lipoplex solution was diluted with ultrapure water to a final volume of 1 mL.

2.2.3 Surface Tension. The surface tension of aqueous solutions of neat surfactants was measured in a Dataphysics DCAT11 tensiometer using the Wilhelmy plate method. The temperature was kept constant at 25.0 ± 0.2 ºC with a thermostated Julabo water bath. The surfactant solutions used for the interfacial characterization were prepared on the same day of the experiment and fresh ultrapure water was used in all samples.

2.2.4 Light Microscopy. An Olympus BX51 light microscope was used for high-contrast video-imaging of vesicle dispersions and for penetration scans of solid samples, using bright field mode with differential interference contrast (DIC), and polarized light mode, respectively. In the penetration scans, the solid is placed between the slide and the cover slip, and then a drop of water is placed at one end of the cover slip and seeps slowly into the film. The lyotropic phase behavior of the surfactant can thus be qualitatively investigated in a simple manner using polarized light.[43] The images were acquired with an Olympus DP71 digital video-camera and processed using the CellA software from the manufacturer.

2.2.5 Cryogenic Scanning Electron Microscopy (cryo-SEM). The sample imaging was performed using a JEOL JSM 6301F high resolution scanning electron microscope, equipped with a Gatan Alto 2500 preparation chamber. The sample is placed in a copper sample-holder and vitrified by plunging into liquid-nitrogen slush from room temperature (20 – 25 ºC). The vitrified sample is then transferred to the preparation chamber to be fractured, sublimated at – 95 ºC (120 s) and coated with Au/Pd (30 s). After this procedure, the sample is transferred to the SEM for visualization. Imaging of 10 mM vesicle dispersions and 5 mM lipoplex dispersions was carried out.

2.2.6 Dynamic Light Scattering (DLS). Particle size and zeta-potential (ζ-potential) were measured with a Malvern ZetaSizer Nano ZS particle analyzer, at 25 ˚C. Disposable polystyrene cuvettes for DLS and U-shaped ζ-potential cuvettes were used. The instrument measures scattering information at 173º, using non-invasive backscatter detection. The Malvern Dispersion Technology Software (DTS) was used, with multiple narrow mode (high resolution) data processing. The size distribution data in Table 2 are expressed in multimodal mean number distributions, after checking the repeatability of at least 5 runs per sample. For ζ-potential, DTS monomodal mode data processing was used.

2.2.7 Ethidium bromide exclusion assay. Fluorescence emission due to ethidium bromide (EtBr) in the region 510-700 nm was monitored in a Perkin Elmer Luminescence L550 spectrofluorimeter (excitation wavelength = 510 nm) immediately after addition of surfactant or surfactant/DOPE aggregates to pre-formed EtBr-DNA complexes. EtBr concentration was maintained six times lower than DNA concentration, to guarantee a proportional fluorescence decrease relative to the amount of cationic surfactant. The results were treated according to a procedure described by Silva et al. [44] All emission spectra were integrated, and the ratio of the areas for dye solutions and standard was determined after subtraction of solvent background. Each fluorescence emission spectrum was fitted into a sum of two log-normal functions, corresponding to the two different environment states of the probe: intercalated in the DNA or dispersed in water. Considering that the fluorescence quantum yield of EtBr in the lipoplex remains constant for all CR(+/-), the percentage of complexed DNA at any given CR(+/-), x, can be obtained from the following expression:

$$\%\ \text{complexed DNA} = \frac{\int I_F(0) - \int I_F(x)}{\int I_F(0)} \times 100 \qquad (2)$$

where $I_F(0)$ and $I_F(x)$ represent the total fluorescence intensity of EtBr for CR(+/-) = 0 (i.e. for a neat DNA solution) and for CR(+/-) = x, i.e. after addition of given aliquot of cationic aggregates to the DNA solution.

3. Results and Discussion

3.1 Physicochemical characterization of the surfactant-water systems

3.1.1 Critical aggregation concentrations. All the gemini surfactants are soluble in water at 25 ºC, but while the amine serine-based gemini and *bis*-quat 12-12-12 give rise to clear transparent solutions, the amide and ester form bluish solutions (already an indication of the presence of much larger aggregates). The interfacial behavior of these solutions was studied by surface tension at this temperature, as shown in Fig. 2. The curves show a marked difference in behavior between the amide and ester compounds, on one hand, and the amine and conventional surfactants, on the other hand. Prior to the plateau that indicates the attainment of a *critical aggregation concentration* (*cac*), the curves for the amide and ester compounds show a first inflection point. As will be shown below in more detail, the ester and amide surfactants are in fact bilayer-forming surfactants that form vesicles down to very low concentrations, while the amine homologue is a micelle-forming surfactant, similarly to 12-12-12.[45] Accordingly, for the amine and conventional bis-quat gemini, the *cac* values correspond to a true *critical micelle concentration*, *cmc*, while for the amide and ester they are instead a *critical vesicle concentration*, *cvc*.[46-51]. The first break point that appears for the ester and amide surfactants may signal the formation of initial small aggregates (either micellar or vesicular), similarly to what has been previously reported for other bilayer-forming surfactants.[48,50-52]

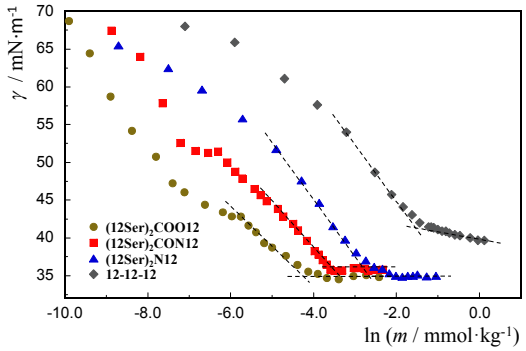

Figure 2. Surface tension versus ln(concentration) curves for the $(12Ser)_2COO12$, $(12Ser)_2CON12$ and $(12Ser)_2N12$ surfactants at 25 ºC. For comparison, the curve obtained for the conventional *bis*-quat gemini 12-12-12 is also shown.

Table 1 shows the interfacial parameters obtained from the γ-ln(m) curves, namely the *cac* (determined as the intersection points in Fig. 2), the surface tension values at *cac*, γ_{cac}, and the minimum surface area per molecule, a_s. The a_s was obtained from the maximum surface excess, Γ_{max}, according to:

$$\Gamma_{max} = -\frac{1}{n\,R\,T}\left\{\frac{\partial\gamma}{\partial \ln(m/m^{\circ})}\right\}_{p,\,T} \quad (3)$$

$$a_s = \frac{1}{N_A\,\Gamma_{max}} \quad (4)$$

where R is the ideal gas constant, T is the absolute temperature, $\partial\gamma/(\partial\ln(m/m^{\circ})$ is the slope of the surface tension plot just below the *cac*, m is the surfactant molal concentration (m° = 1 mmol·kg^{-1}), n is the Gibbs prefactor corresponding to the number of free chemical species at the interface and N_A is the Avogadro constant. The value of n is usually taken as 2 for conventional *bis*-quats, because it is assumed that there is ion pairing and only one of the counterions is dissociated from the ionic headgroup. It has been shown, however, that for a given family of gemini surfactants, n has a subtle dependence on both alkyl chain length and spacer length and ranges from 2 to 3 (i.e. from ion paring to complete dissociation).[53] For these reasons, we present a_s values calculated with both n = 2 and 3, assumed to be the lower and upper bounds. The *cac and* γ_{cac} values are significantly lower for the serine gemini than for 12-12-12, and among the former, for the ester and amide compounds in the case of *cac*. The molecular areas are, however, larger for the two latter compounds. Overall, results show that the serine gemini are more surface-active than the conventional *bis*-quat gemini.

Table 1. Interfacial properties of serine-based gemini surfactants and the homologous conventional *bis*-quat.

surfactants	*cac* / mmol·kg^{-1}	γ_{cac} / mN·m^{-1}	a_s** / nm^2
$(12Ser)_2COO12$	0.014 ± 0.002	35.3	1.47 ± 0.15 (2.20 ± 0.34)
$(12Ser)_2CON12$	0.027 ± 0.004	34.6	1.23 ± 0.09 (1.84 ± 0.21)
$(12Ser)_2N12$	0.077 ± 0.016*	35.8	0.95 ± 0.10 (1.42 ± 0.10)
12-12-12	0.22 ± 0.01*	42.0	0.91 ± 0.11 (1.37 ± 0.11)

*Critical micelle concentrations (*cmc*).
**Values obtained with a Gibbs prefactor n = 2 or, in parenthesis, n = 3.

3.1.2. Spontaneously formed vesicles: structural characterization. To characterize the large aggregates present in the bluish solutions formed by $(12Ser)_2COO12$ and $(12Ser)_2CON12$, both light and cryo-SEM were used. Video-enhanced light microscopy allows the observation of aggregates larger than about 0.5 µm, while the cryo-SEM method used here provides morphological details down to a resolution of ca. 100 nm. As mentioned above, vesicles were observed for these two surfactants. The effect of surfactant concentration (20, 10, 5 and 1 mM) on the vesicle morphology and size distribution was evaluated. Fig. 3 illustrates the observations made, in this case for the $(12Ser)_2CON12$ derivative. Very similar results were obtained for both surfactants (Table 2; cf. also supporting information). Polydisperse vesicles are always seen, with sizes ranging from a few tenths of nm to several µm. These aggregates are responsible for the bluish tint (Tyndall effect) observed macroscopically.

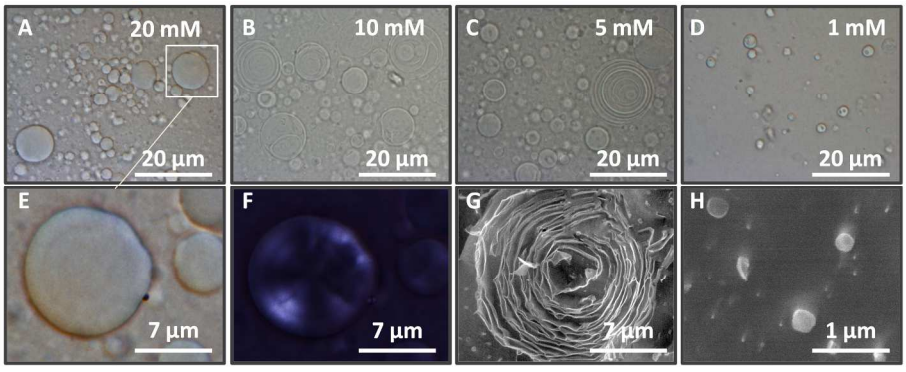

Figure 3. Imaging of $(12Ser)_2CON12$ vesicles: A-D, light micrographs for different surfactant concentrations; E, F, zoom of vesicle in A using (E) unpolarized and (F) polarized light; G and H, cryo-SEM images for 10 mM dispersions showing the presence of both multilamellar (onionsomes) and unilamellar vesicles.

Table 2. Mean hydrodynamic diameter (±SD) and population frequency for the aggregates formed by $(12Ser)_2COO12$ and $(12Ser)_2CON12$, at 25 °C.

	Population A		Population B		Population C	
	D_H / nm	Frequency / %	D_H / nm	Frequency / %	D_H / nm	Frequency / %
$(12Ser)_2COO12$						
20 mM	778 ± 196	83 ± 4	106 ± 21	17 ± 4	---	---
10 mM	845 ± 145	77 ± 1	102 ± 31	17 ± 4	4817 ± 91	6 ± 2
5 mM	829 ± 43	74 ± 1	133 ± 13	19 ± 5	5146 ± 274	7 ± 3
1 mM	750 ± 100	80 ± 4	90 ± 12	15 ± 6	4180 ± 100	5 ± 1
$(12Ser)_2CON12$						
20 mM	874 ± 171	54 ± 4	123 ± 40	11 ± 1	3833 ± 125	35 ± 7
10 mM	877 ± 80	69 ± 5	197 ± 64	20 ± 4	5063 ± 39	11 ± 1
5 mM	767 ± 114	69 ± 1	133 ± 48	19 ± 3	4698 ± 165	12 ± 4
1 mM	798 ± 141	60 ± 6	233 ± 67	34 ± 4	4544 ± 120	6 ± 2

For the most concentrated samples (10 and 20 mM), giant birefringent vesicles are observed. Moreover, cryo-SEM imaging shows the presence of large multilamellar vesicles, in coexistence with small and large unilamellar vesicles. The vesicle size was also followed by DLS and the results obtained (Table 2) are consistent with the microscopy imaging. For all concentrations, three populations of vesicles are observed. Furthermore, one can conclude that for both surfactants upon dilution of the vesicle dispersions in the range 20-1 mM, there is no meaningful change on the size distribution, simply a decrease in the vesicle concentration.

We recall that all four surfactants have a 12-12-12 molecular structure. For the conventional *bis*-quat, the long hydrophobic 12-methylene spacer is known to bend to the inner core of the formed aggregate, with the ultimate result that the surfactant adopts a cone-shaped geometry, i.e. a critical packing parameter[54], P_s, of the order of 0.33, and hence forms small spheroidal micelles.[13,45] It is reasonable to assume that $(12Ser)_2N12$ behaves likewise. However, a plausible explanation for the striking difference in self-assembly for $(12Ser)_2COO12$ and $(12Ser)_2CON12$ can be found in Fig. 1: here the linkage groups form part of the spacers between the charged headgroups (Fig. 1), imparting these molecules with an effectively longer spacer (18 atoms) than in the amine case and a somewhat higher degree of conformational rigidity at the headgroup level. Assuming that the 12-methylene group also bends inwards, the final result is that these gemini adopt a cylindrical geometry at the interface, i.e. a P_s value of the order of ½-1, which favors aggregates with lower mean spontaneous curvature (vesicles). The fact that 12-16-12 (and beyond) conventional bis-quats form vesicles clearly supports this explanation.[13,45]

In order to further confirm the bilayer-forming lyotropic behavior of $(12Ser)_2COO12$ and $(12Ser)_2CON12$, phase penetration scans were performed on the polarized light microscope. For $(12Ser)_2COO12$, as apparent in Fig. 4A, a dilute isotropic solution phase (L) is followed by a lamellar liquid-crystalline phase, L_α, captured by a characteristic focal conics texture. $(12Ser)_2CON12$ also shows a dilute L phase, followed by a L_α phase, characterized by oily streaks and myelin figures (Fig. 4B). This type of phase behavior, dominated by a lamellar phase (the only liquid-crystalline phase present) and, at low concentrations, by a dispersion of vesicular structures, is indeed typical for double-chained surfactants.

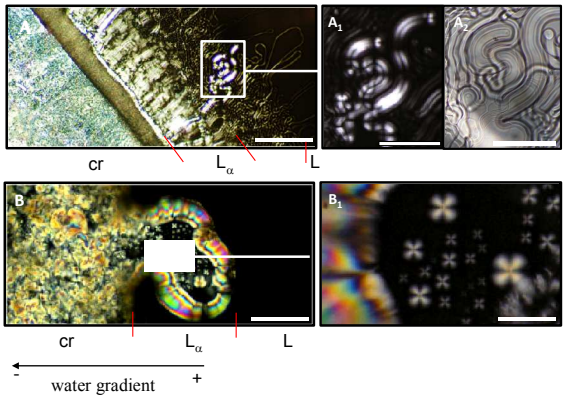

Figure 4. Phase penetration scans: (A) $(12Ser)_2COO12$ (B) $(12Ser)_2CON12$, at 25 °C. Legend: L, isotropic solution phase; L_α, lamellar phase; cr, hydrated crystals. Water is diffusing from right to left into the surfactant crystalline film. Scale bars: A, B - 150 μm; A_1, A_2- 70 μm; B_1- 25 μm.

3.2 DNA compaction studies

3.2.1 Vesicle size control and effect of helper lipid. These cationic gemini surfactants were investigated in terms of their potential to efficiently condense DNA, both *per se* and in mixture with a helper lipid. DNA condensation depends on the electrostatic interaction between DNA phosphate groups and the cationic surfactant headgroups, and on the surfactant packing parameters.[39,41,55] The thermodynamic driving force for lipoplex formation is the direct Coulombic attraction between charges of the two-cosolutes (an enthalpic effect) and the release of counterions from the surfactant aggregate and DNA surface (an entropic effect). The importance of counterion binding in the initial surfactant aggregates is also an important effect than has been highlighted in other works.[17] In our case,

we note that in related gemini serine-based surfactants that form micelles and also have trifluoracetate as counterion, the degree of counterion dissociation was found to be quite high, of the order of 0.6-0.8.[30] Assuming similar situation for the current compounds, electrostatic interactions with DNA for the neat gemini aggregates are favored *ab initio*. The inclusion of DOPE in the cationic aggregate may further favor this interaction since it should weaken the ion binding to the cationic surface and make even more positively charged sites available for DNA binding.[39,41,55] This lipid also tends to form reverse curvature structures that facilitate the transfection process by promoting both membrane fusion and endosomal escape.[37,38]

Firstly, Figure 5 shows that the addition of DOPE in a 1:1 molar ratio to all three serine gemini surfactant systems results in the formation of large polydisperse bilayers structures. Both spherical and deformed elongated vesicles are observed (Fig. 5A, C, and E). Noteworthy is the fact that these non-spherical vesicle structures, a direct effect of DOPE presence, remain stable in solution for a long time, at least for an observation time of two weeks. Moreover, we note that even for the micelle-forming $(12Ser)_2N12$, DOPE with its $P_s > 1$ induces a dramatic decrease in the mean spontaneous curvature of the aggregates and a micelle-to-vesicle transition. If all these mixtures are subject to the extrusion protocol, only small spherical vesicles are present (Fig. 5B and E), in the range of a few tenths of nm to ca. 200 nm.

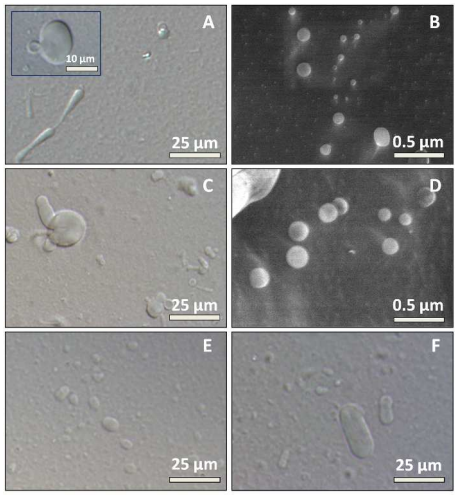

Figure 5. Light and cryo-SEM images for unextruded (A, C and E) and extruded (B and D) gemini/DOPE aggregates: A and B, $(12Ser)_2CON12$/DOPE; C and D, $(12Ser)_2COO12$/DOPE; E, $(12Ser)_2N12$/DOPE.

DLS and zeta-potential (ζ-potential) measurements in Fig. 6 show that the extruded vesicles formed by the serine-based surfactants, with or without presence of DOPE, are stable at least during 15 days. Both the Z-average diameters and zeta-potential (ζ-potential) remain practically constant with values in the range of 110-140 nm (consistent with cryo-SEM) and + 55-60 mV, respectively. Moreover, it is clear that the addition of the helper lipid does not affect the size nor the charge of the extruded vesicles in any significant way.

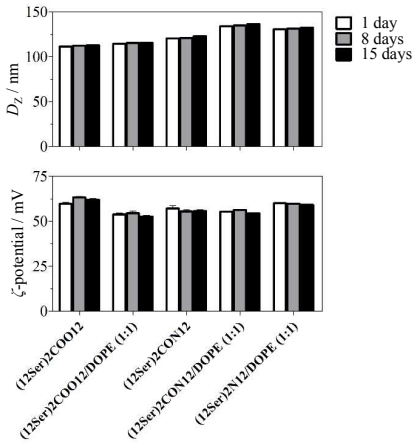

Figure 6. Stability with time of neat gemini and gemini:DOPE vesicles prepared by extrusion: a) size (Z-average diameter); b) ζ-potential.

3.2.2 Lipoplex formation: effect of charge ratio on size distribution and ζ-potential. Lipoplexes were formed by adding increasing aliquots of extruded gemini or gemini/DOPE solutions to a salmon sperm DNA solution, to obtain different CR(+/-) values. Figure 7 shows the mean size and ζ-potential for gemini/DNA and gemini:DOPE/DNA lipoplexes as a function of CR(+/-).

For the single surfactant systems, distinct behaviors are observed. The addition of the $(12Ser)_2CON12$ vesicles to the DNA solution at CR(+/-) = 1:1 and 2:1 gives rise to a precipitate. At higher ratios, however, lipoplexes are formed without any precipitation. As can be seen in Fig. 7a, this surfactant yields the lipoplexes with the highest sizes among the studied systems, ranging from 4 µm, at CR(+/-) = 3:1, to 330 nm, at CR(+/-) = 12:1. Similarly, the $(12Ser)_2N12$ system also precipitates in the presence of DNA, from CR(+/-) = 1:1 to 3:1. Above 3:1, the lipoplexes formed are smaller when compared to those of $(12Ser)_2CON12$, and from 10:1 onwards, the average size is 170 nm. A significant observation is that in the case of $(12Ser)_2COO12$ no precipitation was detected within the observation time (24 hrs) and CR(+/-) range. The lipoplex size stabilizes from CR(+/-) = 6:1 onwards, with an average value of 160 nm. An explanation for these differences in behavior of the amine and amide systems on hand (precipitation) and the ester system on the other (no precipitation) is not straightforward, but one can put forth some hypotheses. Several factors that favor precipitation can be at stake for the former two surfactants, such as a higher degree of counterion dissociation for the initial aggregates[17] and/or a more favorable matching between the positive charge-to-charge distance in the headgroups and the DNA phosphate-to-phosphate distance (≈ 7 Å).[7,10] With respect to the much smaller lipoplexes found for $(12Ser)_2N12$ than for $(12Ser)_2CON12$, a simple explanation could be that micelles are the initial aggregates present for the amine compound, while vesicles are

present for the amide one, and this may determine the final size of the lipoplexes.

The incorporation of DOPE inhibits precipitation in all gemini systems, in contrast with what was observed for the neat amide and amine derivatives at low CRs. Moreover, DOPE seems to bring significant advantages with respect to the lipoplex sizes, since the latter are smaller at charge ratios significantly lower than for the respective neat gemini system (Fig. 7a). The differences in the compaction profile, in the absence and presence of DOPE, are more visible for the $(12Ser)_2N12$ and $(12Ser)_2CON12$ derivatives than for the $(12Ser)_2COO12$. For all gemini/DOPE systems, from CR(+/-) = 3:1 onwards, the lipoplexes have an average size between 110 and 170 nm.

Cryo-SEM imaging of some of the lipoplex solutions prepared (Fig. 8) are in line with the results from DLS (smaller aggregates with DOPE present, at lower CR values). Moreover, they suggest that at least for the CR(+/-) checked, the vesicular structure is preserved upon DNA complexation, since no other type of aggregates could be observed.

The ζ-potential value indirectly reflects the lipoplex surface net charge and can therefore be used to evaluate the extent of interaction of the cationic aggregate with DNA. As the CR(+/-) increases, an increase in ζ-potential relative to that of neat DNA (-30 mV) is observed (Fig. 7b). The isoelectric point (neutral charge, zero ζ-potential) occurs at charge ratios higher than equimolarity for all the gemini/DNA and gemini:DOPE/DNA, except for the $(12Ser)_2COO12$ and $(12Ser)_2COO12$/DOPE systems, which reach the isoelectric point at CR(+/-) < 1. All lipoplexes are positively charged for CR ≥ 2:1. This type of behavior, i.e., the reaching of the isoelectric point in lipoplexes for CR(+/-) larger than 1 is relatively common, having been reported for other systems.[10,17,56] Besides the influence of counterion binding on effective aggregate surface charge, another possible explanation is that, assuming that the lipoplexe microstructure is still vesicular and that the initial vesicles do not suffer breakage and major rearrangements upon DNA binding, then part of the charge, the one in the inner monolayer of the vesicles, is not effectively available for interaction.

In the presence of DOPE, several relevant differences are apparent. For the $(12Ser)_2CON12$ and $(12Ser)_2COO12$ derivatives, the ζ-potential values are less positive than those for the lipoplexes based on the neat surfactants. The $(12Ser)_2CON12$ derivative lipoplexes reach a plateau around CR(+/-) = 3:1 and at ~ +35 mV, while for the $(12Ser)_2COO12$ derivative a clear plateau is not attained, with the ζ-potential ranging from +25 to +40 mV. This decrease in ζ-potential in DOPE presence can be understood if one considers that dispersed phosphatidylethanolamine aggregates per se have been found to be slightly negatively charged, despite the zwitterionic nature of the lipid headgroup[57]. Hence, in principle, mixed DOPE:gemini vesicles should be less positively charged than neat gemini vesicles (as indeed found, Fig. 6); this will also be reflected in the lipoplexes' charge. For $(12Ser)_2N12$, a different behavior is found: here the DOPE-containing lipoplexes are more positively charged than the neat gemini lipoplexes. With DOPE, a plateau is reached at CR(+/-) = 3:1 and ζ = +50 mV. This seems to be a surprising result at first sight, but we should bear in mind that neat $(12Ser)_2N12$ forms micelles while the $(12Ser)_2N12$:DOPE mixture forms vesicles. The vesicle aggregates most certainly have higher ζ-potential than the micelles and this could also be reflected in the lipoplex morphology and charge.

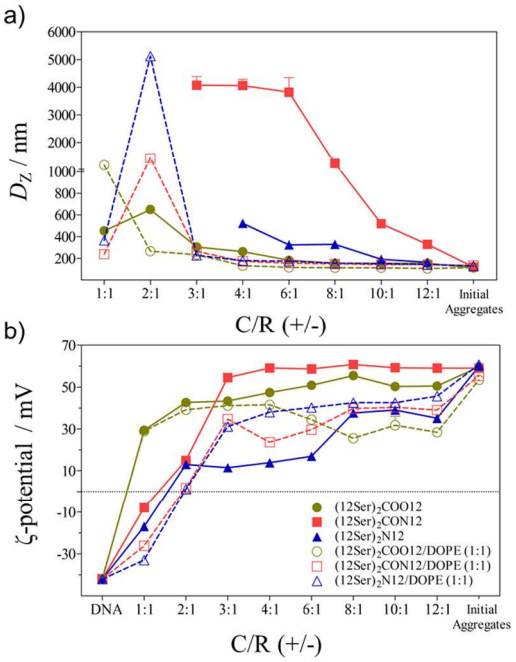

Figure 7. Neat gemini and gemini/DOPE lipoplexes: a) mean size and b) ζ-potential as a function of surfactant/DNA charge ratio (+/-). The symbols are identical for both a) and b).

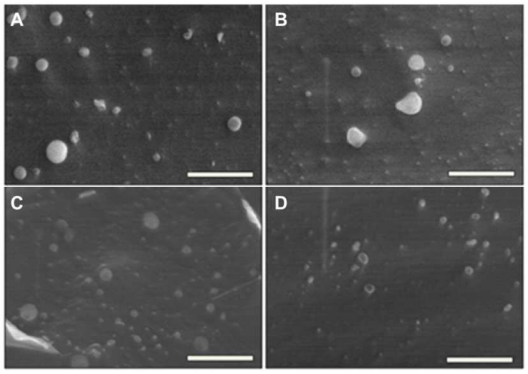

Figure 8. Cryo-SEM imaging for neat gemini and gemini/DOPE lipoplexes, at 5 mM and different charge ratios: A, $(12Ser)_2COO12$ CR(+/-) = 12:1; B, $(12Ser)_2COO12$/DOPE CR(+/-) = 4:1; C, $(12Ser)_2CON12$ CR(+/-) = 6:1; and D, $(12Ser)_2CON12$/DOPE CR(+/-) = 4:1. Scale bars: 0.6 μm. In all micrographs, vesicular structures are present.

Regarding neat serine derivatives, the $(12Ser)_2CON12$ lipoplexes have the highest ζ-potential values, +55 mV from CR(+/-) = 3:1 onwards. The $(12Ser)_2N12$ lipoplexes attain a first

plateau at +15 mV, between CR(+/-) = 2:1 – 6:1, and at higher CRs the ζ-potential is close to +35 mV. For the $(12Ser)_2COO12$ lipoplexes, the ζ-potential plateau is reached at CR(+/-) = 2:1 and the values vary within +42 and +50 mV up to CR(+/-) = 12:1. It should be pointed out that size and ζ-potential measurements were performed within 4-5 hours of lipoplex preparation, for all systems studied. Furthermore, the lipoplexes, above isoelectric point, are stable at least for 24 hours, with no meaningful variation being observed in both size and ζ-potential values. Therefore, even in cases where they may be kinetically trapped non-equilibrium structures instead of equilibrium ones, their metastability is long enough to allow for transfection studies to be carried out.

3.2.3 DNA compaction profile. The ability of the cationic serine aggregates to compact DNA was also assessed by the ethidium bromide, EtBr, exclusion assay. Ethidium bromide is a fluorophore which interacts with DNA by intercalating itself between the adjacent base pairs in the double helix. When intercalated, EtBr fluoresces at 610 nm by direct excitation at 510 nm. However, upon condensation by cationic aggregates, the probe is displaced from the DNA to the aqueous solution and a decrease in fluorescence is observed. EtBr fluorescence is approximately 30-fold higher when intercalated between the DNA bases compared to its fluorescence in water.[58, 59]

Fig. 9 shows the normalized fluorescence intensity, $I_F/I_{F,max}$, of EtBr as a function of the gemini/DNA and gemini:DOPE/DNA charge ratio, at 25 ˚C and at constant DNA concentration. Fig. 10 shows the corresponding curves of percentage of complexed DNA *versus* charge ratio for the same systems.

For the neat gemini lipoplexes, the decrease in probe fluorescence reaches a plateau for $I_F/I_{F,max}$ = 0.05 (displacement of 95 % EtBr) at CR(+/-) = 3:1 for the amide and ester derivatives, and at CR(+/-) = 2:1 for the amine derivative, pointing to differences in the complexation process of the different gemini systems. Thus, lipoplexes formed by the amine derivative compact the same amount of DNA at charge ratios slightly lower than for the other two surfactants. This observation may be related with the fact that the starting aggregates in the case of the amine surfactant are small micelles, whereas for the other surfactants they are vesicles. Micelles are much smaller aggregates than vesicles (about two orders of magnitude) and hence the system has higher surface area available for interaction with DNA anionic charges. Moreover, in the case of vesicles part of the charge is in the inner monolayer and, as mentioned before, unless the vesicles are significantly disrupted in the process, such charge will not be easily available. Therefore, in the case of vesicles, higher charge ratio (i.e. higher amount of surfactant) is needed for the same degree of complexation to take place.

For all the systems tested, the increase in CR(+/-), and consequently the increase of gemini or gemini/DOPE content with respect to DNA in the lipoplex, results in a considerable raise in DNA compaction, as inferred from the reduction of EtBr fluorescence, due to its displacement from DNA.

In the case of the gemini/DOPE systems, one must bear in mind first that the starting aggregates, i.e. the aggregates existing prior to DNA condensation, are mixed vesicles, as supported by DLS and cryo-SEM (Fig. 5). Furthermore, there should be now a charge dilution effect owing to the presence of the uncharged lipid in the bilayer structure. Despite these features in common, the three systems do not behave in the same fashion upon interaction with DNA. As can be seen in Fig. 9b, the amide surfactant-containing system shows the sharpest decrease in fluorescence intensity with increasing CR(+/-), attaining a plateau at 2:1, with a very high compaction efficiency (~99%, Fig. 10). In contrast, the inclusion of DOPE into the ester and amine gemini causes a much slower decrease in fluorescence intensity with increasing CR(+/-) (Fig. 9b). For these mixtures a CR(+/-) = 8:1 is necessary to attain a plateau in $I_F/I_{F,max}$, which corresponds to a 93% compaction efficiency (Fig. 10).

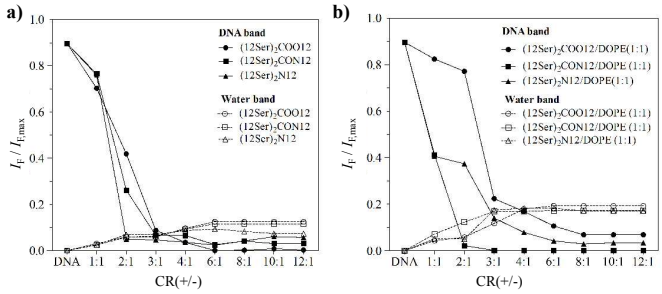

Figure 9. EtBr exclusion assay for: a) neat gemini and b) gemini/DOPE lipoplexes. The fluorescence intensity curves have been decomposed, with each EtBr fluorescence emission spectrum fitted to a sum of two log-normal functions, corresponding to different environments (DNA and water).

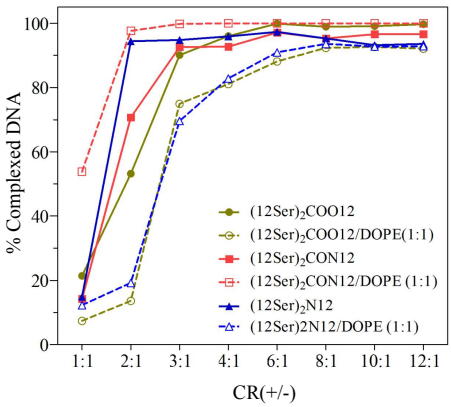

Figure 10. Percentage of complexed DNA for neat gemini and gemini/DOPE lipoplexes, at different charge ratios.

Even though the results and comparisons herein described are rather interesting, a more in-depth rationalization of the effects behind them would require a fine structural study of the lipoplexes formed at different CR(+/-). With respect to potential transfection efficiency of these lipoplexes, one must first recognize that this ability depends not only on the structural features of the lipoplexes *per se*, namely size, charge

and morphology, but also in other factors, such as cell types, inclusion of helper lipids, *in vitro* or *in vivo* conditions, hence making the scenario somewhat complex.[6-11,60,61] While small lipoplexes (< 100 nm) seem to be essential for efficient *in vivo* delivery, larger ones (200–400 nm) are optimal for *in vitro* transfection. Large lipoplexes seem to be advantageous when endocytosis is the dominant cell internalization mechanism but for non-endocytic paths, either small particles perform better or no obvious size/transfection efficiency correlation is found.[60,61] Another relevant property is the zeta potential of the lipoplexes, and while the majority of successful lipoplexes are positively charged ($\zeta \approx$ 30-40 mV), it is also a fact that complexes with a negative zeta potential have also been reported as efficient in gene delivery.[10,60]

Bearing in mind all these confluent factors for optimal transfection efficiency, and on the basis of our results, we can hypothesize that in the absence of DOPE, the $(12Ser)_2COO12$-based lipoplexes are *a priori* the best candidates for testing *in vitro* DNA transfection since they have in combination high DNA-binding (> 90%) at relatively low +/- charge ratio ($\geq$ 3:1), relatively low sizes (< 400 nm) and moderate ζ-potential ($\approx$ +40 mV). For the gemini:DOPE lipoplexes, and along the same line of reasoning, the optimal candidate could be $(12Ser)_2CON12$:DOPE lipoplexes, as they show high binding ($\approx$95%) at CR(+/-) $\geq$ 3:1, 200-300 nm in size and $\zeta \approx$ +35 mV. However, it is clear that these assumptions have to be tested and, as if often the case with transfection efficiency, *a posteriori* rationalization from a physicochemical standpoint is required.

4. Conclusions

The interfacial properties and self-assembly behavior of the three gemini surfactants (12Ser)2N12, $(12Ser)_2CON12$ and $(12Ser)_2COO12$ were investigated. Most notorious was the fact that the amide and ester derivatives spontaneously form vesicles, while the amine derivative forms micelles. The *cac* values are much lower than for the conventional gemini analogue. A significant result is that all the compounds were found to efficiently compact DNA, either as neat surfactants or in binary mixtures with DOPE. While for the amine and ester derivatives DNA compaction was more efficient for the single systems, in the case of the amide derivative, the inclusion of DOPE significantly enhanced compaction efficiency. As previously noted, the lipoplexes size decreases as the CR(+/-) increases until it reaches a plateau. The neat gemini surfactants have distinct behaviors, with the ester derivative forming lipoplexes of smaller size at lowest charge ratios (CR = 6:1, 160 nm). The amide derivative yields the largest lipoplexes. Typically, with the inclusion of DOPE, beyond a charge ratio of 3:1 a plateau is reached, with lipoplexes having a similar size as the initial aggregates (about 110-170 nm). All the lipoplexes are positively charged from CR(+/-) = 2:1 onwards, and for the neat amide and ester derivatives the highest ζ-potential values are attained (+ 50-60 mV). All mixtures show very high compaction efficiency, more than 90% of complexed DNA. Hence, both gemini and gemini/DOPE lipoplexes seem to be promising systems for transfection assays.

5. Acknowledgements

This work was supported by research projects PTDC/QUI-QUI/115212/2009 and PTDC/QUI-BIQ/103001/2008 and through the re-equipment program REDE/1517/RMN/2005 funded by the Portuguese Foundation for Science and Technology (FCT) and FEDER-Compete. MLCV and EFM are also grateful to CIQUP for financial support through projects Pest/C-QUI/UI0081/2011 and Pest/C-QUI/UI0081/2013. SGS acknowledges financial support from FCT and European Social Fund (ESF) under the Community Support Framework (CFS) through PhD grant SFRH/BD/61193/2009. The authors also kindly acknowledge Profs. Eulália Pereira and Paula Gameiro, REQUIMTE, Department of Chemistry and Biochemistry of Faculty of Science, University of Porto, for the access to the Zeta sizer and spectrofluorimeter used in this work.

Notes

Affiliation: Centro de Investigação em Química, Department of Chemistry and Biochemistry, Faculty of Science, University of Porto, Rua do campo Alegre s/n, P 4169-007 Porto, Portugal.

Electronic Supplementary Information (ESI) available. See DOI: 10.1039/b000000x/

References

1. G. Cevc, *Adv. Drug Deliv. Rev.*, 2004, **56**, 675-711.
2. A. S. Ulrich, *Bioscience Rep.*, 2002, **22**, 129-150.
3. L. Yang and P. Alexandridis, *Curr. Opin. Colloid Interface Sci.*, 2000, **5**, 132-143.
4. X. Zhang and C. Wang, *Chem. Soc. Rev.*, 2011, **40**, 94-101.
5. M. Malmsten, *Soft Matter*, 2006, **2**, 760-769.
6. A. J. Kirby, P. Camilleri, J. B. F. N. Engberts, M. C. Feiters, R. J. M. Nolte, O. Söderman, M. Bergsma, P. C. Bell, M. L. Fielden, C. L. García Rodríguez, P. Guédat, A. Kremer, C. McGregor, C. Perrin, G. Ronsin and M. C. P. Van Eijk, *Angew. Chem. Int. Ed.*, 2003, **42**, 1448-1457.
7. S. D. Wettig, R. E. Verrall and M. Foldvari, *Curr. Gene Ther.*, 2008, **8**, 9-23.
8. C. Bombelli, L. Giansanti, P. Luciani and G. Mancini, *Curr. Med. Chem.*, 2009, **16**, 171-183.
9. M. Donkuru, I. Badea, S. Wettig, R. Verrall, M. Elsabahy and M. Foldvari, *Nanomedicine*, 2010, **5**, 1103-1127.
10. A. M. S. Cardoso, H. Faneca, J. A. S. Almeida, A. A. C. C. Pais, E. F. Marques, M. C. P. De Lima and A. S. Jurado, *BBA-Biomembranes*, 2011, **1808**, 341-351.
11. E. Junquera and E. Aicart, *Curr. Top. Med. Chem.*, 2014, **14**, 649-663.
12. F. M. Menger and J. S. Keiper, *Angew. Chem. Int. Ed.*, 2000, **39**, 1906-1920.
13. R. Zana, *Adv. Colloid Interface Sci.*, 2002, **97**, 205-253.

14. L. Karlsson, M. C. P. Van Eijk and O. Söderman, *J. Colloid Interface Sci.*, 2002, **252**, 290-296.
15. M. Muñoz-Úbeda, S. K. Misra, A. L. Barrán-Berdón, S. Datta, C. Aicart-Ramos, P. Castro-Hartmann, P. Kondaiah, E. Junquera, S. Bhattacharya and E. Aicart, *Biomacromolecules*, 2012, **13**, 3926-3937.
16. S. Bhattacharya and A. Bajaj, *Chem. Comm.*, 2009, 4632-4656.
17. C. Wang, X. Li, S. D. Wettig, I. Badea, M. Foldvari and R. E. Verrall, *Phys. Chem. Chem.Phys.*, 2007, **9**, 1616-1628.
18. A. R. Tehrani-Bagha and K. Holmberg, *Langmuir*, 2010, **26**, 9276-9282.
19. J. A. S. Almeida, E. F. Marques, A. S. Jurado and A. A. C. C. Pais, *Phys. Chem. Chem. Phys.*, 2010, **12**, 14462-14476.
20. J. A. S. Almeida, S. P. R. Pinto, Y. Wang, E. F. Marques and A. A. C. C. Pais, *Phys. Chem. Chem. Phys.*, 2011, **13**, 13772-13782.
21. S. M. C. Silva, J. J. S. Sousa, E. F. Marques, A. A. C. C. Pais and B. B. Michniak-Kohn, *AAPS J.*, 2013, **15**, 1119-1127.
22. H. Lv, S. Zhang, B. Wang, S. Cui and J. Yan, *J. Control. Release*, 2006, **114**, 100-109.
23. A. Colomer, A. Pinazo, M. A. Manresa, M. P. Vinardell, M. Mitjans, M. R. Infante and L. Pérez, *J. Med. Chem.*, 2011, **54**, 989-1002.
24. F. M. Menger and B. N. A. Mbadugha, *J. Am. Chem. Soc.*, 2001, **123**, 875-885.
25. M. Johnsson and J. Engberts, *J. Phys. Org. Chem.*, 2004, **17**, 934-944.
26. T. Yoshimura, K. Ishihara and K. Esumi, *Langmuir*, 2005, **21**, 10409-10415.
27. L. Wasungu, M. Scarzello, G. Van Dam, G. Molema, A. Wagenaar, J. B. F. N. Engberts and D. Hoekstra, *J. Mol. Med.* 2006, **84**, 774-784.
28. J. Singh, P. Yang, D. Michel, R. E. Verrall, M. Foldvari and I. Badea, *Curr. Drug Deliv.*, 2011, **8**, 299-306.
29. S. G. Silva, C. Alves, A. M. S. Cardoso, A. S. Jurado, M. C. Pedroso De Lima, M. L. C. Vale and E. F. Marques, *Eur. J. Org. Chem.*, 2013, 1758-1769.
30. S. G. Silva, R. F. Fernandes, E. F. Marques and M. L. C. Do Vale, *Eur. J. Org. Chem.*, 2012, 345-352.
31. L. Pérez, A. Pinazo, R. Pons and M. Infante, *Adv. Colloid Interface Sci.*, 2014, **205**, 134-155.
32. M. Damen, E. Cristóbal-Lecina, G. C. Sanmartí, S. F. M. Van Dongen, C. L. García Rodríguez, I. P. Dolbnya, R. J. M. Nolte and M. C. Feiters, *Soft Matter*, 2014, **10**, 5702-5714.
33. C. Zheng, L. Niu, W. Pan, J. Zhou, H. Lv, J. Cheng and D. Liang, *Polymer*, 2014, **55**, 2464-2471.
34. M. Ramezani, M. Khoshhamdam, A. Dehshahri and B. Malaekeh-Nikouei, *Colloids Surf. B*, 2009, **72**, 1-5.
35. M. Radwan Almofti, H. Harashima, Y. Shinohara, A. Almofti, Y. Baba and H. Kiwada, *Arch. Biochem. Biophys.*, 2003, **410**, 246-253.
36. N. J. Zuidam, D. Hirsch-Lerner, S. Margulies and Y. Barenholz, *BBA-Biomembranes*, 1999, **1419**, 207-220.
37. S. W. Hui, M. Langner, Y. L. Zhao, P. Ross, E. Hurley and K. Chan, *Biophys. J.*, 1996, **71**, 590-599.
38. M. Muñoz-Úbeda, S. K. Misra, A. L. Barrán-Berdón, C. Aicart-Ramos, M. B. Sierra, J. Biswas, P. Kondaiah, E. Junquera, S. Bhattacharya and E. Aicart, *J. Am. Chem. Soc.*, 2011, **133**, 18014-18017.
39. L. Wasungu and D. Hoekstra, *J. Control. Release*, 2006, **116**, 255-264.
40. S. Zhang, Y. Xu, B. Wang, W. Qiao, D. Liu and Z. Li, *J. Control. Release*, 2004, **100**, 165-180.
41. M. C. Pedroso De Lima, S. Simões, P. Pires, H. Faneca and N. Düzgüneş, *Adv. Drug Deliv. Rev.*, 2001, **47**, 277-294.
42. F. H. Stephenson, *Calculations for Molecular Biology and Biotechnology*, Academic, London, 2010.
43. A. S. C. Lawrence, *Mol. Cryst.* 1969, **7**, 1-57.
44. J. P. N. Silva, P. J. G. Coutinho and M. E. C. D. R. Oliveira, *J. Fluoresc.*, 2008, **18**, 555-562.
45. D. Danino, Y. Talmon and R. Zana, *Langmuir*, 1995, **11**, 1448-1456.
46. T. F. Svitova, Y. P. Smirnova, S. A. Pisarev and N. A. Berezina, *Colloids Surf. A*, 1995, **98**, 107-115.
47. E. F. Marques, O. Regev, A. Khan, M. D. Miguel and B. Lindman, *J. Phys. Chem. B*, 1999, **103**, 8353-8363.
48. J. F. A. Soltero, F. Bautista, E. Pecina, J. E. Puig, O. Manero, Z. Proverbio and P. C. Schulz, *Colloid Polym. Sci.*, 2000, **278**, 37-47.
49. P. del Burgo, E. Aicart, O. Llorca and E. Junquera, *J. Phys. Chem. B*, 2006, **110**, 23524-23539.
50. B. V. Shankar and A. Patnaik, *Langmuir*, 2007, **23**, 3523-3529.
51. Z. Jiang, J. Liu, K. Sun, J. F. Dong, X. F. Li, S. Z. Mao, Y. R. Du and M. L. Liu, *Colloid Polym. Sci.*, 2014, **292**, 739-747.
52. I. Grillo, J. Penfold, I. Tucker and F. Cousin, *Langmuir*, 2009, **25**, 3932-3943.
53. P. X. Li, C. C. Dong, R. K. Thomas, J. Penfold and Y. Wang, *Langmuir*, 2011, **27**, 2575-2586.
54. J. N. Israelachvili, D. J. Mitchell and B. W. Ninham, *J. Chem. Soc., Faraday Trans. 2*, 1976, **72**, 1525-1568.
55. D. D. Lasic and N. S. Templeton, *Adv. Drug Deliv. Rev.*, 1996, **20**, 221-266.
56. J. P. N. Silva, A. C. N. Oliveira, M. P. P. A. Casal, A. C. Gomes, P. J. G. Coutinho, O. P. Coutinho and M. E. C. D. R. Oliveira, *BBA-Biomembranes*, 2011, **1808**, 2440-2449.
57. R. Willumeit, M. Kumpugdee, S. S. Funari, K. Lohner, B. P. Navas, K. Brandenburg, S. Linser and J. Andrä, *BBA-Biomembranes*, 2005, **1669**, 125-134.
58. J. R. Lakowicz, *Principles of Fluorescence Spectroscopy*, 3rd ed., Springer-Verlag, New York, 2006.
59. P. C. A. Barreleiro and B. Lindman, *J. Phys. Chem. B*, 2003, **107**, 6208-6213.
60. B. Ma, S. Zhang, H. Jiang, B. Zhao and H. Lv, *J. Control. Release*, 2007, **123**, 184-194.
61. I. S. Zuhorn, J. B. F. N. Engberts and D. Hoekstra, *Eur. Biophys. J.*, 2007, **36**, 349-362.

